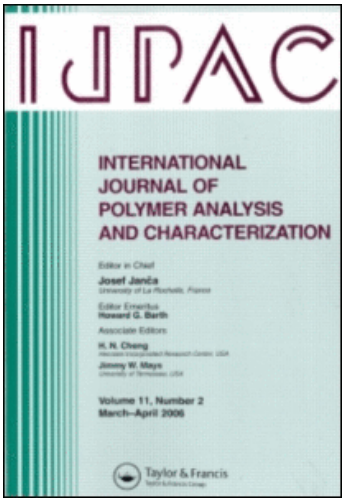

International Journal of Polymer Analysis and Characterization
Publication details, including instructions for authors and subscription information:
http://www.informaworld.com/smpp/title~content=t713646643

Assessment of Linearity Conditions in Thermal Field-Flow Fractionation by Peak Shape Analysis

Pierluigi Reschiglian[a]; Michel Martin[b]; Catia Contado[c]; Francesco Dondi[c]
[a] Department of Chemistry ,G. Ciamician', University of Bologna, Bologna, Italy [b] École Supérieure de Physique et de Chimie Industrielles. Laboratoire de Physique et Mécanique des Milieux Hétérogènes (URA CNRS 857), Paris, Cedex 05, France [c] Department of Chemistry, University of Ferrara, Ferrara, Italy

To cite this Article Reschiglian, Pierluigi , Martin, Michel , Contado, Catia and Dondi, Francesco(1997) 'Assessment of Linearity Conditions in Thermal Field-Flow Fractionation by Peak Shape Analysis', International Journal of Polymer Analysis and Characterization, 3: 2, 107 — 130
To link to this Article: DOI: 10.1080/10236669708032758
URL: http://dx.doi.org/10.1080/10236669708032758

Int. J. Polymer Analysis & Characterization
1997, Vol. 3, pp. 107–130
Reprints available directly from the publisher
Photocopying permitted by license only

Assessment of Linearity Conditions in Thermal Field-Flow Fractionation by Peak Shape Analysis

PIERLUIGI RESCHIGLIAN*

Department of Chemistry "G. Ciamician", University of Bologna, via Selmi 2, I-40126 Bologna, Italy

MICHEL MARTIN

École Supérieure de Physique et de Chimie Industrielles. Laboratoire de Physique et Mécanique des Milieux Hétérogènes (URA CNRS 857) 10 rue Vauquelin, 75231 Paris Cedex 05, France

CATIA CONTADO and FRANCESCO DONDI*

Department of Chemistry, University of Ferrara, via L. Borsari 46, I-44100 Ferrara, Italy

(Received 9 October 1995; In final form 5 March 1996)

Linearity conditions in thermal-field flow fractionation, which are required for unambiguous results, are dealt with by a numerical and graphical peak shape analysis approach. Nonlinear effects, such as injected sample overloading as a function of sample concentration and field strength, can be detected by the Edgeworth-Cramér (EC) peak shape fitting method and the determination of relative statistical peak parameter determination. The physical implication of the nonlinearity effect is also discussed. Peak retention parameters by numerical integration are determined and the differences obtained by means of the above methods are compared.

Keywords: Thermal field-flow fractionation (ThFFF), peak shape analysis, Edgeworth-Cramér method

*Corresponding author.

INTRODUCTION

Thermal field-flow fractionation (ThFFF), which is a technique belonging to the family of field-flow fractionation (FFF) methods, is capable of measuring the molecular weight distribution (MWD) of a wide variety of organo-soluble polymers [1]. As compared to size-exclusion chromatography (SEC), ThFFF methods often exhibit higher separation selectivity for MWD determination [2]. ThFFF separations typically use a single solvent and take place when a large thermal gradient is applied across a very thin ribbon-like spacer from which the channel volume is removed. This strip is sandwiched between two bare polished metal blocks. The thermal gradient generally pushes sample components toward the cooler metal block (*accumulation wall*) and the flow profile generated within the channel results in a steep velocity profile of the flow streams near the wall. For the most known polymer/solvent systems, the higher molecular weight (MW) components are pushed closer to the accumulation wall and are swept down the channel by slower flow streams and elute after lower-MW components [3]. The result is a fractogram that closely resembles an SEC chromatogram with a reversed elution order, that is the highest MW components elute last in ThFFF. The combination of thermal field and longitudinal, laminar flow makes it possible to classify ThFFF, as in classical chromatography, as a separation technique with perpendicular field and flow axes [4].

One of the most important features of ThFFF is that fractograms can be used to determine the MWD from which average molecular weights and polymer polydispersity μ are derived. Several methods were suggested for this purpose [5–10]. However, the accuracy of ThFFF-based MW data is markedly dependent on the experimental conditions in which unbiased retention parameter values can be attained. That no interactions occur between sample molecules is among the assumptions reported for the standard retention equation in FFF [4]. These assumptions are actually a necessary condition for a chromatographic process to be defined as *linear*. As long as the behavior remains linear, peak parameters of the elution profile are independent of concentration.

Sample overloading was first reported as one of the most important sources of nonlinearity in FFF and concentration effects, in terms of retention parameters and peak shape distortion, were studied in ThFFF [11,12], although neither a quantitative study of the complete peak shape analysis nor an accurate estimate of the higher-than-first order moments has yet been reported for polymer fractionation by ThFFF.

Nonetheless, the onset of nonlinear effects and secondary-order phenomena has been studied in sedimentation field-flow fractionation (SdFFF) by peak shape analysis [13]. It is well known, in fact, that peak fitting methods are more accurate than integration methods, which suffer from the uncertainty in fixing the baseline to obtain statistical peak parameters [14].

This study experimentally evaluates nonlinearity effects on ThFFF retention through a complete peak shape analysis by means of the Edgeworth-Cramér (EC) series fitting method [14–17]. A comparison is made using different methods of estimating peak parameters (i.e., mean and standard deviation): numeric integration and the EC series peak fitting are checked with respect to their ability to monitor the effect changing experimental conditions (field strength and injected sample concentration) has on peak shape parameters. Necessary conditions for linearity (NCL) are verified by EC series fitting for the analysis of polystyrene (PS) standards in ethylbenzene (EB). The results of the present study should prove useful in two ways: first, to establish practical rules for performing ThFFF measurements under conditions of vanishing, small nonlinearity effects; second, to set up an unambiguous and quantitative numerical-graphical method for the evaluation of separate experimental effects in more extended systematic investigations.

THEORY

EC Series Peak Shape Fitting

Theoretical basis of the EC series expansion and the ability to approximate peaks under linear conditions have already been reported for the chromatographic process interpreted as a stochastic process with stationary and independent increments [18,19]. It is, thus, likely that the above property holds true also for a chromatographic-like process as for FFF migration. Theory and applications of EC fitting for detecting nonlinearity effects in chromatography and SdFFF have been described elsewhere [13,17].

Peak shape analysis is performed by the EC least-squares fitting of the experimental ThFFF peak $Y_{sp}(x)$. The EC series are obtained according to the method defined by Edgeworth [20]:

$$Y_{sp}(x) = y(x)A/\sigma \tag{1}$$

$$y(x) = y_K(x) + r_K(x) \tag{2}$$

$$y_K(x) = Z(x) + \sum_{v=1}^{K} Q_v(-Z) \tag{3}$$

where A is the peak area; x is the well-known Gaussian, normalized time variable $x = (t - m)/\sigma$, where m is the peak mean, t the time and σ the standard deviation; $y_K(x)$ is the EC series expansion developed up to the Kth term; $Q_v(-Z)$ is a linear aggregate of the derivatives of the Gaussian frequency function $Z(x)$, maximum order 3υ, and contains the cumulant coefficients γ_υ, of maximum order υ, of the frequency function $y(x)$; $r_K(x)$ is the normalized remainder [13]. An EC series expansion development up to the Kth term can generate a theoretically computed peak Y_{cal} which is, thus, expressed as:

$$Y(x)_{cal,K} = y_K(x)A/\sigma \tag{4}$$

For a given K expansion, the nonlinear least-squares EC fitting can be expressed as:

$$\min \sum [(Y_{sp,i} - Y_{cal,K,i})100/Y_{\max}]^2 = \min \sum \Delta^2_{K,i}\% \tag{5}$$

where the minimum is reached with respect to the peak parameter set (A, m, σ and γ_1 to $\gamma_K)_K$, where $\gamma_1, \ldots \gamma_K$ are the cumulant coefficients and Y_{max}, $Y_{sp,i}$, $Y_{cal,K,i}$ are the peak height, the experimental and the EC fitted peak profile, at the time point t_1, respectively. In practice, the EC series fitting procedure consists of a stepwise increase of the expansion order K in Equation (5) (and related Equations (3) and Equations (4)) up to a maximum K value (K_{max}) as in the well-known polynomial least-squares fitting procedure, until the best statistically meaningful approximation is reached. The stepwise fitting process must satisfy four rules (well-behaved fitting rules), whose simultaneous consistency is a necessary condition for a linear process (NCL) [16]:

1) The maximum expansion order K is related to the degree of peak skewness and signal-to-noise ratio [16].
2) The parameter set (A, m, σ and γ_1 to $\gamma_K)_K$ for a given fitting pattern is stable as K is increased to its maximum value [14–17].
3) The mean approximation, expressed as:

$$(CV\%)_K = [(\sum \Delta^2_{K,i}\%/(N_p - n_p - 1)]^{1/2} \tag{6}$$

where N_p and n_p are respectively the number of points and the number of parameters and Y_{max} the peak height, lowers as K is increased.

4) For the fitting residuals $\Delta_{k,i}$ % the number of nodes (*i.e.*, the number of points where $\Delta_{K,i}$ % = 0) increases as the K degree is raised. Moreover, the fitting residuals are almost symmetrical with respect to $x = 0$ [14].

The approximation degree of a peak can also be estimated by the approximation-to-noise ratio (*ANR*) parameter, which can be expressed as:

$$ANR_K = (CV\%)_K \frac{S/N}{25} \tag{7}$$

where *S/N* is the signal-to-noise ratio [21]. Since *ANR* also accounts for the intrinsic system noise, *ANR* values express the inability of the EC series to approximate the experimental peak more clearly than does *CV%*.

The simultaneous consistency of the four above-mentioned rules for well-behaved fitting defines the NCL for a chromatographic process. Such an approach has proved to be very sensitive and much more stringent with respect to concentration effects than are peak height measurements for different separation techniques, such as GC in packed and capillary columns and ion chromatography [17,22,23]. However, the NCL discussed above might not be *sufficient*, under some specific occurrences, to prove linearity. For instance, a particular nonlinear condition leading to a distinct peak distortion can apparently be fitted under conditions of well-behaved EC series fitting. The behavior is followed in the transition zone from highly nonlinear conditions—producing very distorted peak shapes—to linear conditions which are, indeed, limiting conditions holding true only at vanishing small concentrations.

Peak Parameters Analysis

Among the peak parameters from an EC fitting output, the first two cumulant coefficients are most usually referred to as peak shape parameters [24]:

$$\gamma_1 = S = \frac{m_3}{\sigma^3} \tag{8}$$

$$\gamma_2 = E = \frac{m_4}{\sigma^4} - 3 \tag{9}$$

where m_3 and m_4 are the third and fourth central moments, respectively. The S and E parameters are the skewness and the excess and express the degree of peak asymmetry and flattening, respectively. From an EC series fitting, a useful peak attribute is achievable:

$$X_0 = \Delta t/\sigma \tag{10}$$

$$X_0 \cong -(1/2)S \tag{11}$$

X_0 is the mode normalized coordinate and represents the difference Δt between the elution time of the peak maximum t_{max} and the retention time, defined as the elution time of the peak barycenter t_r [24]. By combining Equations (10) and (11) one gets:

$$(\Delta t/t_{\max})\% = -100(1/2)S\sigma/t_{\max} \tag{12}$$

MW Determination

For FFF in general, as in other liquid chromatographic techniques, the most characterizing elution parameter is the retention ratio R, which can be expressed as:

$$R = \frac{V_0}{V_r} = \frac{t_0}{t_r} \tag{13}$$

where V_0 is the dead volume, V_r the elution volume of the sample, and t_0 the void time.

For most FFF systems for which the flow profile can be assumed to be parabolic, R is accurately related to the mean layer thickness of the migrating band l and to the channel thickness w as follows:

$$\lambda = \frac{l}{w} \tag{14}$$

$$R = 6\lambda[\coth(1/2\lambda) - 2\lambda] \tag{15}$$

For ThFFF, λ is approximated by:

$$\lambda = \frac{D}{D_T \Delta \mathrm{T}} \tag{16}$$

where ΔT represents the temperature difference across the channel and D and D_T are the coefficients for ordinary and thermal diffusion, respectively

[1]. The ordinary diffusion coefficient D can be expressed by the relation:

$$D = \frac{A}{M^b} \tag{17}$$

where A and b are constants for the polymer/solvent system at a given temperature and which have previously been reported for PS/EB [7]. By substituting Equation (17) into Equation (16), and with the experimental values of λ from retention ratios R, one gets the polymer MW as [25]:

$$M = \left(\frac{A}{\lambda D_T \Delta T}\right)^{\frac{1}{b}} \tag{18}$$

If peak maxima rather than peak means are used for MW determinations, by combining Equations (12), (13), (15) and (18) one gets a functional expression of the relative error on MW determination with respect to the nominal MW ($(\Delta M/M)\%$) as:

$$(\Delta M/M)\% = f((\Delta t/t_{max})\%, A, b, D_T, \Delta T) \tag{19}$$

EXPERIMENTAL

The ThFFF system used in this work was the model T100 ThFFF Polymer Fractionator (FFFractionation, LLC, Salt Lake City, UT, USA). It consists of two copper bars with highly polished faces clamped together over a polyimide spacer with nominal thickness of 0.0127 cm. The actual thickness was measured once the channel had been opened after performing the experiments. The thickness was 0.0139 ± 0.0006 cm, as determined with a micrometer by sampling the polyimide strip all around the channel. The other channel dimensions were 1.9 cm in breadth by 45.6-cm long with tapered ends. The hot bar was heated by two 3-kW electrical cartridge heaters controlled by an A/D board-linked PC. The cold bar had three holes drilled the entire length, allowing coolant to enter through the central hole and exit through the outer holes. Both the top and the bottom bars had small holes for temperature measurement by thermistors.

The solutions of polymer samples were injected by means of an injector with a 20-μL loop (Rheodyne, model 7125). After the injection, flow was stopped and samples were allowed to relax for 1 min to achieve their equilibrium position. A model 420 HPLC pump (Kontron Instruments S.p.A., Milan,

Italy) was used to supply carrier flow. The carrier solvent was extrapure EB 03080 (Fluka Chemic. A.G., Buchs, Switzerland). Peak detection was achieved with a model R410 Refractive Index Detector (Waters Associates, Milford, MA, USA). Void volume was 1.39 ± 0.02 mL which was determined by injecting tetrahydrofuran (J.T. Baker B.V., Deventer, The Netherlands) as the unretained probe. The total external dead volume resulting from the difference between experimental (1.39 mL) and geometric channel volume was 0.025 mL. This value was unusually large with respect to the minimized dimensions of the connection tubes employed in all the experiments and it was ascribable to the RI detector cell, in which the cell had been built with a long capillary tube spooled inside the cell housing for best temperature stability.

The sample was narrow-monodisperse linear polystyrene standard (μ = 1.04) (Polymer Laboratories Ltd., Church Stretton, U.K.) (reported MW = 170,000, μ = 1.04, batch *N*° 20137-2)

COMPUTATIONAL

Data collection from the ThFFF system was driven by a software package routine from FFFractionation Inc. The routine also included a Savitsky-Golay (S.G.) smoothing procedure by which digitized raw fractograms were filtered before EC fitting. The Y_t experimental data were taken as absolute values since RI differential detection of PS in EB gave a negative output signal. Both the baseline and linear drift were subtracted by linear interpolation of those points flanking the peak mean by a range of normalized variable units spanning around $\pm 5\sigma$. The nonlinear least-squares fitting was initiated by using the zeroth-order EC series term, the Gaussian function. The EC series least-squares fitting was a FORTRAN compiled software run on a cloned AT-compatible 80386 PC. The general minimizing routine [26] integrated into the EC series package required the minimized function values and its gradients, as described in ref. [13]. The EC series least-squares fitting routine also includes the computation of first peak moments by integration.

RESULTS AND DISCUSSION

In the present study, two experimental variables affecting the peak parameters and shapes have been considered: sample concentration from 0.5% w/v to 2.5% w/v and field strength from $\Delta T = 35$°C to $\Delta T = 60$°C.

EC Series Analysis of Retention Parameters

Figure 1a reports a series of superimposed fractograms of the PS sample: the complex peak shape deformations obtained with increasing injected concentrations are clearly shown. In Figure 2, the best EC curve fit of the least skewed peak obtained at low field strength ($\Delta T = 40°C$) and low sample load (1%) is shown together with its own single components (*1*, *2*, *3*): a slight but appreciable distortion is evident once the experimental peak is compared to its normal component ($Z(x)$), even at low injected concentrations. Table I reports the numerical results of peak shape analysis for the PS sample under different field strengths ΔT and loads (% w/v). In Figure 1b, the R and plate height H parameters are reported as a function of the injected concentration. Comparison of Figures 1a and b and Figure 2 shows that EC series fitting experiments prove highly accurate in monitoring any peak shape difference, even for almost Gaussian profiles.

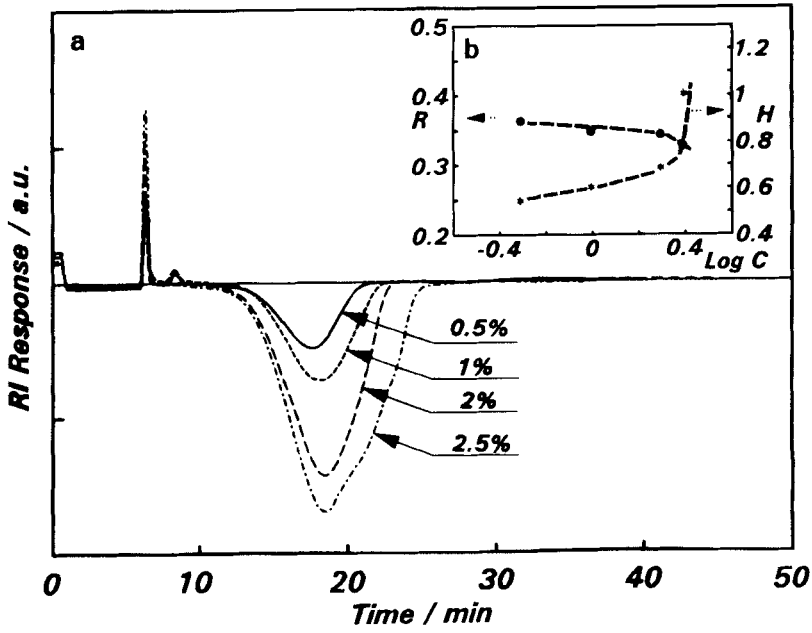

FIGURE 1 a) Comparison between PS experimental fractograms at different injected concentrations (% *w/v*), ΔT = 45°C; b) Dependence of the relative retention ratio R and plate height H values on the injected concentration (*log c*).

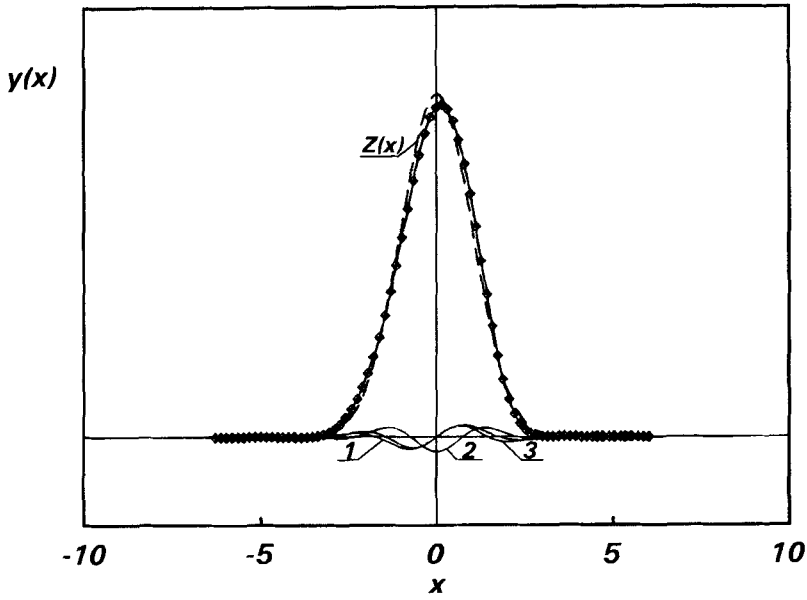

FIGURE 2 EC fifth-order approximation: single peak components, 170,000 g/mol PS, 1% w/v, ΔT = 40°C; solid line = experimental peak; +++ = fitted peak; dashed line = Gaussian component ($Z(x)$), *1* = $Q_1(-Z)$, *2* = $Q_2(-Z)$, *3* = $Q_3(-Z)$ (see Equation (3)).

TABLE I Peak parameters by EC peak-shape fitting[a].

% w/v	[3]ΔT	R	[1]H	S	E	K_{max}	[2]S/N	$CV\%$	[2]ANR
1	35	0.420	0.64	−0.17	−0.23	5	451	0.18	5.24
1	40	0.377	0.58	−0.14	−0.29	5	337	0.16	3.76
1	45	0.345	0.60	−0.26	−0.19	6	400	0.34	7.67
1	50	0.317	0.54	−0.28	−0.56	5	387	0.65	10.69
1	60	0.288	0.41	−0.84	1.32	3	279	0.62	8.04
0.5	40	0.394	0.57	−0.40	0.18	4	373	0.27	4.33
0.5	45	0.361	0.54	−0.46	0.29	5	280	0.14	2.12
2	40	0.374	0.75	−0.27	−0.39	6	441	0.43	8.1
2	45	0.342	0.68	−0.47	−0.26	4	414	0.73	12.9
2.5	40	0.357	1.04	−0.35	−0.26	5	665	1.34	35.93
2.5	45	0.326	1.00	−0.28	0.13	5	510	1.19	26.87

[a]Sample 170,000 g/mol PS, 0.2 mL/min flow rate; [1]Values determined from the normal component (cm)
[2]Values from non smoothed peaks; [3]ΔT in °C.

In Table I, the statistical peak parameters, signal-to-noise ratio (*S/N*), coefficient of variation of the fitting (*CV%*) (Equation (5)) and approximation-to-noise ratio (*ANR*) (Equation (7)) are listed for the series expansion order of the best fitting (K_{max}). *ANR* and *S/N* values were obtained from non-smoothed peak fittings. High *ANR* values express the progressive inability of the EC series to approximate peaks at increasing sample loads and field strengths. *ANR* is lower than *ca.* 10–15, indeed, only when the concentration is below 2% w/v and ΔT below 45°C (see Table I). A progressive decrease in R is also observed with an increase in sample load (from R = 0.394, 0.5% at 40°C to R = 0.357, 2.5% at 40°C; from R = 0.361, 0.5% at 45°C to R = 0.326, 2.5% at 45°C) as well as an increase in H (*e.g.* see Figure 1b for ΔT = 45°C). It should be noted that the extent of the decrease of R (*ca.* 10%) with injected amount is meaningful since the estimated precision level [16] on the R determination by EC series fitting is *ca.* 1% in the present experimental conditions. These findings give evidence of an overloading onset which yields effects similar to those already described as resulting in shifts toward smaller R and increases in band broadening with increasing concentration [11,12,27]. The observed depression of R values above 0.5% w/v should not be considered as ascribable to the instrumental unsteadiness in maintaining the chosen ΔT. Indeed, variations in temperature readings never exceeded the nominal instrumental specifications of ±1 °C. The observed decrease in R does not, however, agree with other experimental observations of an increase in R with increasing sample loads for somewhat different polymer/solvent systems analyzed in field programming conditions [9]. A possible explanation of the observed dependence of R on sample load is given below.

Physical Implication of Concentration Effects in ThFFF

The observed dependence of R is likely due to several sources. Sample overloading may affect the retention factor through three transport parameters: the viscosity, which affects the diffusion coefficient and the field-induced velocity which, in ThFFF, is proportional to the thermal diffusion coefficient D_T. The viscosity is increased near the wall where the polymer accumulates, thus the relative velocity near the wall in the polymer zone is lower than at infinite dilution and this effect alone tends to decrease R. The gradient diffusion coefficient of the polymer, which is the coefficient to be considered in the establishment of the equilibrium

concentration profile, increases with increasing polymer concentrations. This was shown to be true for PS in toluene [28–33] and one can reasonably expect it is also true for PS in EB. This influence tends to increase the mean thickness of the polymer cloud near the accumulation wall and to repel the solute toward the fast moving streamlines in the channel center. The effect of the influence of the concentration on the diffusion coefficient is thus opposite to that of the viscosity since it tends to increase R.

A recently developed theoretical model of retention in SdFFF at finite concentrations [34] predicts that the retention ratio R of hard spheres should increase with increasing concentrations, in agreement with experimental findings with aqueous suspensions of rigid particles of polystyrene latex [13,35]. The differential overloading effects on retention of rigid particles by SdFFF and of polymers by ThFFF may arise from a difference between the variations of the sedimentation velocity and those of D_T with sample concentrations. While the relatively strong decrease of the sedimentation velocity with increasing concentrations is well documented, there are large variations reported in the literature on the dependence of D_T for PS in toluene with the concentration [29,36–39]. However, it might well happen that different behavior, with regard to concentration effects, between polymers in ThFFF and particles in SdFFF is associated not with the technique used but with sample type. Indeed, the retention time of polymers (PS/EB) by flow FFF has been seen to increase with increasing concentrations [11] while the opposite effect was found, in qualitative agreement with the hard sphere SdFFF model, for proteins in asymmetrical flow FFF [40] and polystyrene latex in flow FFF with hollow fibers [41]. This specific behavior of polymeric samples may possibly be due to chain entanglement of two or more macromolecules, which would reduce diffusivity and enhance the viscosity of the entangled polymers, thus increasing their retention. This last point will be discussed further with regard to the specific conditions used in this work.

Linearity Characterization by EC Series Peak Shape Analysis

Since depression in R values with increasing sample load may prove the onset of nonlinear effects on retention, the stringency of linearity conditions was tested with respect to the well-behaved fitting rules whose simultaneous consistency has been defined under the theory section as a necessary, although not sufficient condition for a linear process. Figures 3a and 3b and Figure 4 report the *CV%* fitting patterns for different sample

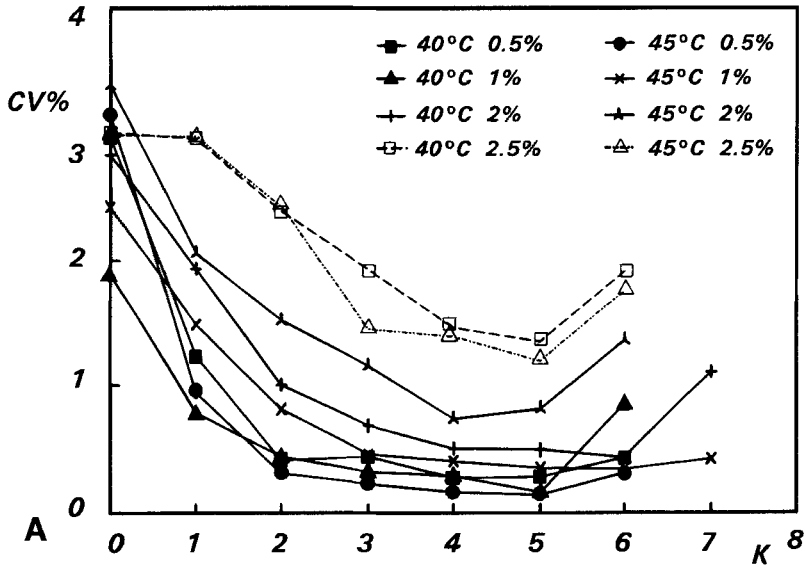

FIGURE 3a Relative approximation error *CV%* as a function of the EC series expansion order *K*; dependence on sample loading at different field strengths.

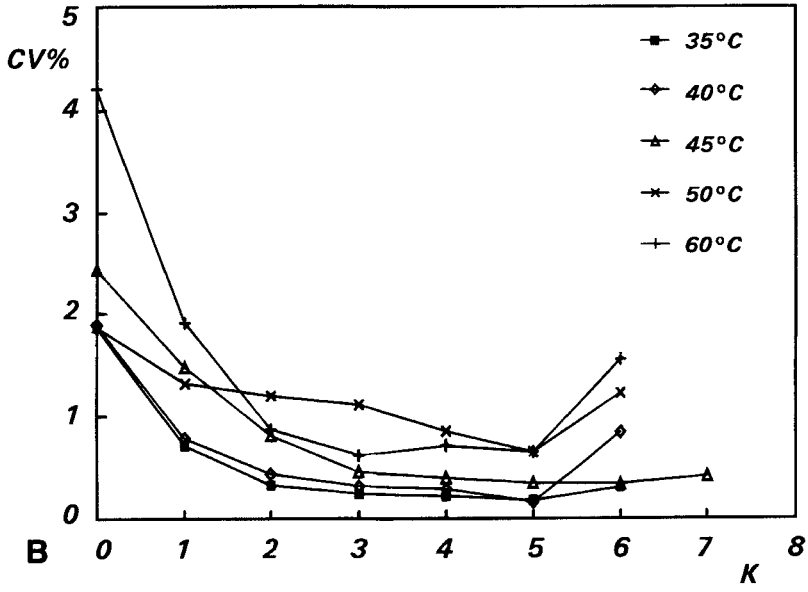

FIGURE 3b Relative approximation error *CV%* as a function of the EC series expansion order *K*; dependence on field strength, sample load: 1% w/v.

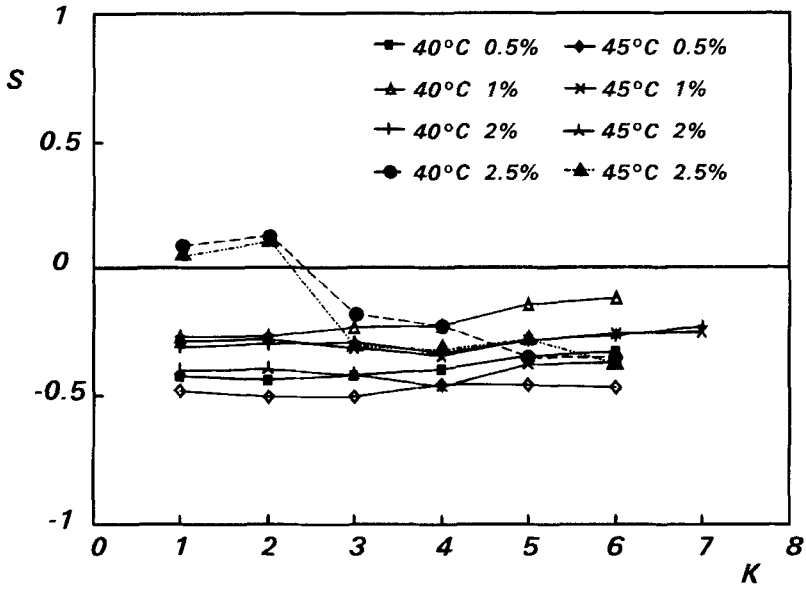

FIGURE 4 Skewness S versus EC series expansion order K; dependence on sample loading at different field strengths.

loads, different field strengths and the S pattern for different sample loads, respectively. It can be observed from the $CV\%$ patterns (Figures 3a and 3b) that the best fitting conditions are rapidly obtained below 1% w/v sample load and $\Delta T = 45°C$, even with EC series expansion *ca.* $K = 2$. In these cases, no further fitting improvement by expanding more and more the EC series up to $K_{max} = 5$ is actually achieved. On the contrary, at higher load and field strengths, the fitting minimum is always worse than in the previous cases and it is just gradually attained at $K_{max} \approx 5$. This finding not only reflects the lack of the EC series ability to approximate peak shape as the injected concentration is increased, but it also indicates an increase in the number of parameters required to account for the changed peak shape on increasing the injected concentration. In practice, the first two cumulant coefficients, S and E, see Equations (8) and (9), are sufficient up to 1% w/v injected concentration, whereas the high-order cumulants γ_3, γ_4 and γ_5 are not even sufficient to represent the more deformed shapes. This feature depicts the image of the complex deformations observed in the fractograms by means of the EC series, as shown in Figure 1a. This feature was confirmed by detailed fitting patterns of the parameter set (see *rule 2*). As

shown for the S pattern at high load (2.5% w/v) (Figure 4), it was indeed observed that rule 2 was not obeyed at the highest field strength (ΔT = 60°C) either.

The main question arising from these findings lies in whether—or, better, to what extent—the behavior can be assumed as linear below the reported concentration and field strength. The latter point is critical, indeed, for any chromatographic-like elution experiment since the exact, reference peak shape with respect to which one can compare experimental peaks (*e.g.*, by a X^2 test) is not yet theoretically available. Therefore, the only approach to the above question lies in detecting the peak shape variations within the set of experimentally accessible data. This approach can be better explained by referring to Table I, where the peak parameter values derived from the ultimate EC series expansion K_{max} are reported for different field strength and injected concentration conditions. The concentration effect on peak parameters can be analyzed at two thermal gradient values (ΔT = 40°C and ΔT = 45°C) in the concentration range 0.5–2% w/v, the 2.5% w/v case being defined as nonlinear, as explained above (rule 2 not followed). As far as the R values are concerned, a slow, yet distinctly increasing trend (± 5%) is observed upon decreasing the injected concentration value. At the same time, the H values decrease, even if the relative difference between the data at 1% w/v and at 0.5% w/v is not higher than 10% (see Figure 1b). Otherwise, *ANR* values indicate very good fitting results for sample loads within 1% w/v. Therefore, on the basis of such an analysis, one can reasonably state that, at injected concentrations equal or lower than 1% w/v, the region behaves as almost linear. However, as the effect of the injected concentration on S and E is analyzed, more significant fluctuations, even between 0.5 and 1% w/v, were observed (see Table I). However, further exploitation of concentration levels lower than those here examined was not considered because of the instability of the baseline due to the various drift sources in the experimental system. EC series fitting is sensitive to baseline instability even if EC is superior and more robust than integration methods [14]. The point of accurately exploiting even lower concentration domains would call for further investigation and instrumentation improvements.

The occurring dependence of both the S and E trends upon the concentration value is uncertain and difficult to analyze, although it is quite distinct: for instance, a common inversion can be observed for the E parameter, from negative (*ca.* –0.2) to positive values (*ca.* +0.25), both for

$\Delta T = 40°C$ and $\Delta T = 45°C$, with the injected concentration decreasing from 1% to 0.5% w/v. However, the apparently dramatic change observed in the E parameter must be thought of as, indeed, very modest in terms of shape effects and real change of the 4th moment value, E being a quantity scaled by the standard value of 3 (see Equations (9)). The observed feature may be due to the ability of the overall peak profile to maintain some early shape distortions experienced as the band migration process begins, or, most likely, during the relaxation process, when the band concentration is still high, whereas the same effect has minor relevance on the main parameters R and H.

As far as the dependence on field strength is concerned, if one compares the effects reflected in the peak parameters to those due to sample loading there is evidence that an increase in ΔT acts as the onset of a type of overloading phenomena in which a decrease in mean layer thickness, resulting from an increased compression of the sample layer at the accumulation wall, can be expected to cause the same type of nonidealities as those observed when increasing sample load [11]. However, a full exploitation of these effects would require more extended experimental design which is beyond the aims of the present paper. A summary of the physical sources of the observed peak shape deformations is reported below.

The possibility that the concentration near the accumulation wall c_0 becomes larger than the critical concentration c^* separating the dilute regime (in which molecules behave individually) from the semidiluted regime (in which polymer coils are entangled) cannot only account for the progressive increase in retention but also for the change in peak shape attributes with increasing sample load and/or field strength, possibly due to the formation of microgels. For the PS 170,000 MW/EB system, c^*, which can be approximated by the reciprocal of the intrinsic viscosity, becomes equal to 1.58×10^{-2} g/mL. The samples at 2% and 2.5% w/v already exceed this value before injection. Nevertheless, even for the most diluted sample (0.5% w/v), c_o at the channel inlet (calculated as $c_{inj}/\lambda = 5.7 \times 10^{-2}$ at $\Delta T = 40°C$ where c_{inj} is the injected sample concentration [11]), is far above c^*. This finding might also explain the slight departure (fronting) from ideality observed even at the lowest sample loads used in the present study.

A graphic study is a more direct way to represent the performed peak shape analysis. In Figures 5–6, a comparison of experimental S.G.-smoothed peaks, corresponding EC fitted profiles and relative normal components, all normalized at unit area, is shown for different sample loads and

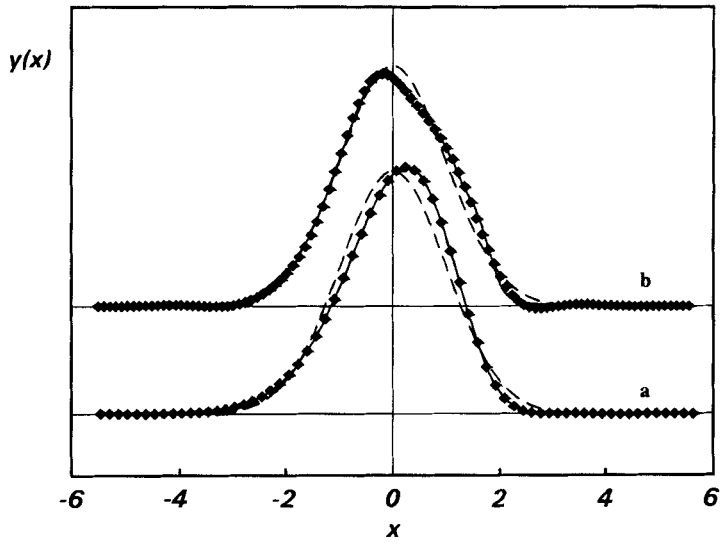

FIGURE 5 Normalized experimental (full line), EC fitted (symbols), and relative Gaussian component (dashed line) peaks *vs* normalized time variable (x) at different sample loads. a) 170,000 g/mol PS, 0.5% w/v $\Delta T = 45°C$; b) 170,000 g/mol PS, 2.5% w/v $\Delta T = 45°C$.

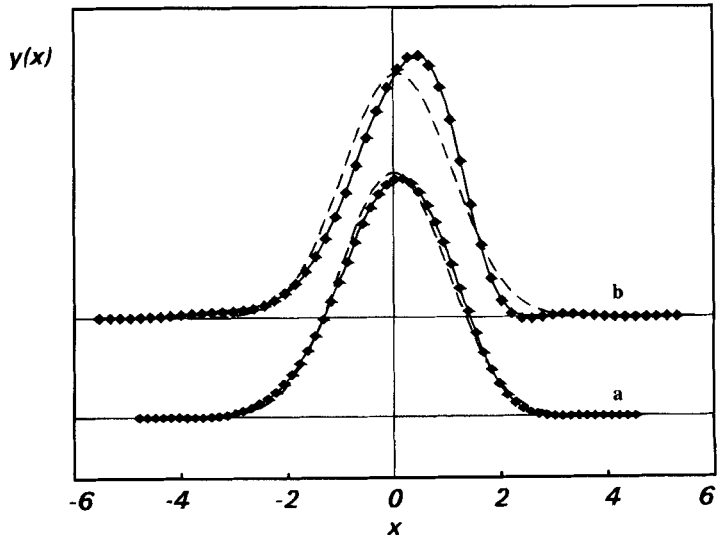

FIGURE 6 Normalized experimental (full line), EC fitted (symbols), and relative Gaussian component (dashed line) peaks vs. normalized time variable (x) at different field strengths; sample load = 1% w/v. a) 170,000 g/mol PS, $\Delta T = 35°C$; b) 170,000 g/mol PS, $\Delta T = 60°C$.

field strengths, respectively. Peaks do not maintain the same shape, as perceived through the patterns in Figures 3–4. At the highest sample load (Figure 5b), there is clearly peak distortion with a shoulder that may indicate the onset of artifact peaks.

The lack of the EC series to approximate peaks eluted under nonlinearity conditions is also clearly seen in the absolute values, as well as in the oscillatory nature of the fitting residual function expressed as $D\%$, as shown in Figures 7–8, which refer to the fittings of Figures 5–6, respectively. In the cases which were recognized in the limits of linearity on the basis of the main peak parameter (R, H) stability discussed above, the degree of fitting is not only good but also homogeneous over the whole peak with a large number of nodes (Figures 7–8a). This last finding agrees with rule 4 defined under the theory section. On the contrary, it can clearly be seen in Figures 7–8b that rule 4 does not hold true for those experimental conditions which stand beyond the limiting values for linearity derived from the fitting pattern analysis.

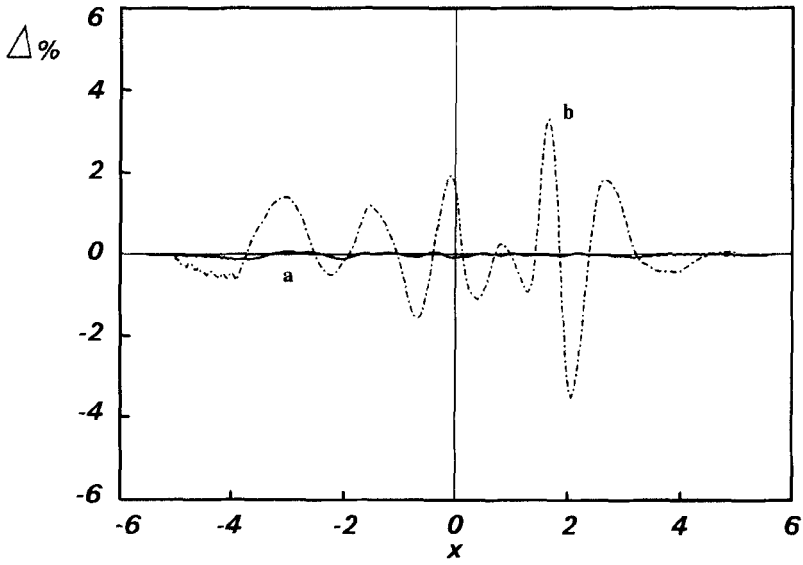

FIGURE 7 Residuals of EC series fitting. Δ% = percent differences between fitted and experimental peak a) (full line) 170,000 g/mol PS, 0.5% w/v, ΔT = 45°C; b) (dashed line) 170,000 g/mol PS, 2.5% ΔT = 45°C.

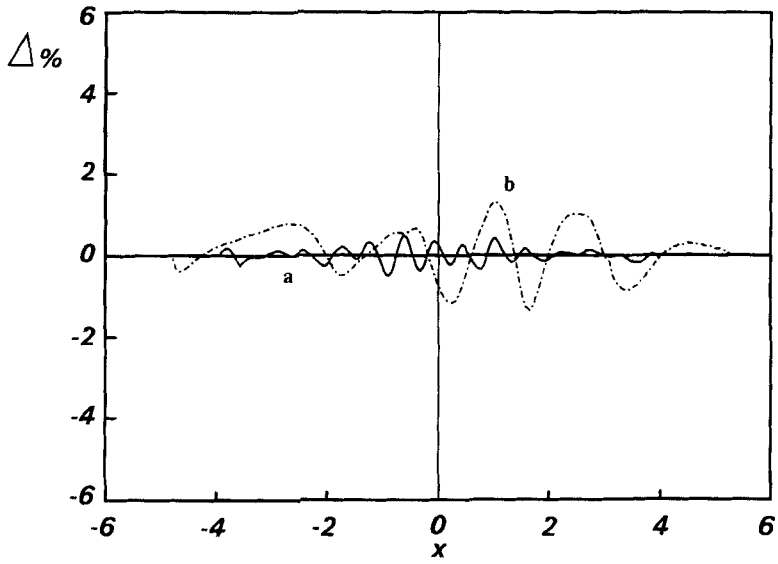

FIGURE 8 Residuals of EC series fitting. Δ% = percent differences between fitted and experimental peak; a) (full line) 170,000 g/mol PS, 1% w/v, ΔT = 35°C; b) (dashed line) 170,000 g/mol PS, 1% ΔT = 60°C.

Peak Shape Markers for Detecting the Nonlinearity Extent

The application of the EC peak-shape analysis for detecting nonlinearity effects in ThFFF gives a coherent picture of the onset of nonlinearity, which indeed appears as a complex continuous process detectable at various degrees. In fact, it has been shown that one can identify different nonlinearity indicators given by the EC series procedure itself. It can also be proved that nonlinearity markers make it possible to detect nonlinearity effects at various sensitivity levels as follows:

1st level: Changes in S and E indicate a marginal nonlinearity that is revealed even at the lowest concentrations and ΔT values.

2nd level: The onset of significant detectable changes in R and H with an increase in the injected concentration diagnoses the first real onset of nonlinearity.

3rd level: On further increasing the injected concentration, there is a progressive lack of the EC series fitting ability below the critical level (*ANR* values as high as *ca.* 5–10), together with an increase in the number of cumulants needed for the peak shape approximation.

4th level: A clear nonlinearity with peak shape artifacts is indicated by the breakdown of the peak parameter stability with increasing K (well-behaved fitting rule 2 not followed), together with an abnormal behavior of the fitting residuals (well-behaved fitting rule 4 not followed).

Comparison Between Different Numerical Methods for Peak Parameters Determination

A comparison between the features obtained by EC peak-shape analysis and those that can be attained by other more conventional methods is considered in more detail. In Tables II–III, two sets of retention parameter values derived from calculation based on integration and EC peak shape fitting analysis are reported at various field strengths and different sample loads,

TABLE II Peak asymmetry effects from fitting and integration analysis: effect of the field strength.

		EC parameters				Integration parameters		
% w/v	$^{1}\Delta T$	S	$^{a}X_0$	$^{b}(\Delta t/t_{max})$ %	$^{c}(\Delta M/M)$ %	$^{2}\Delta t$	$^{b}(\Delta t/t_{max})$ %	$^{c}(\Delta M/M)$ %
1	35	–0.17	0.08	0.96	2.16	7	0.84	1.95
1	40	–0.14	0.07	0.76	1.49	8	0.86	1.85
1	45	–0.26	0.13	1.47	3.15	14	1.37	2.75
1	50	–0.28	0.14	1.54	3.30	10	0.91	1.97
1	60	–0.84	0.42	3.93	7.98	46	3.69	7.51

Experimental sets: [a]Values obtained by Equation (11), [b]Values obtained by Equation (12), [c]Values obtained by Equations (18) and (15), $A = 2.613 \times 10^{-4}$, $b = 0.552$ and $D_T = 0.95 \times 10^{-7}$ [$cm^2 s^{-1} K^{-1}$] [7], $^{1}\Delta T$ values are expressed in centigrades, $^{2}\Delta t$ is expressed in s.

TABLE III Peak asymmetry effects from fitting and integration analysis: effect of the sample load.

		EC parameters				Integration parameters		
% w/v	$^{1}\Delta T$	S	$^{a}X_0$	$^{b}(\Delta t/t_{max})$ %	$^{c}(\Delta M/M)$ %	$^{2}\Delta t$	$^{b}(\Delta t/t_{max})$ %	$^{c}(\Delta M/M)$ %
0.5	40	–0.4	0.2	2.21	4.92	26	2.87	6.26
0.5	45	–0.46	0.23	2.54	5.41	25	2.54	5.41
1	40	–0.14	0.07	0.76	1.49	8	0.86	1.85
1	45	–0.26	0.13	1.47	3.15	14	1.37	2.75
2	40	–0.27	0.13	1.69	3.63	21	2.22	4.71
2	45	–0.47	0.23	2.89	6.01	21	2.03	4.16
2.5	40	–0.35	0.18	2.71	5.74	–15	–1.56	–3.49
2.5	45	–0.28	0.14	2.22	4.69	–26	–2.51	–5.37

Experimental sets: [a]Values obtained by Equation (11), [b]Values obtained by Equation (12), [c]Values obtained by Equations (18) and (15), $A = 2.613 \times 10^{-4}$, $b = 0.552$ and $D_T = 0.95 \times 10^{-7}$ [$cm^2 s^{-1} K^{-1}$] [7], $^{1}\Delta T$ values are expressed in °C, $^{2}\Delta t$ is expressed in s.

respectively. Integration values are the input conditions for the fitting procedure (*i.e.*, $K = 0$) and were calculated as described under the computational section. Consistency between integration and numerical EC peak shape fitting is monitored by comparing the differences in retention times between fitted peak maxima and normalized time variable origins (peak means), as well as the retention time error ($(\Delta t/t_{max})\%$) reached by using peak maximum rather than peak mean. In Table III, significant discrepancies between EC and integration parameters (from negative to positive values) are observed only for the highest sample loads where EC series fitting ability drops at the onset of nonlinearity. In particular, the Δt values obtained by integration are consistent with those calculated from S by EC fitting through the parameter X_0 (Equation (10)) only within the limits for NCL which were defined above. Therefore, the retention time error reached by using the peak maximum rather than the peak mean (Equation (12)), and thus the derived relative error on MW determination with respect to the nominal MW ($\Delta M/M$)% (Equation (19)), is consistent between EC fitting and integration methods within the onset of nonlinearity.

It can also be observed that only at the highest field strength for a modest sample load (Table II, 1% w/v $\Delta T = 60\%$) does the ($\Delta M/M$)% value significantly rise above 5%. As far as a comparison between peak parameter determination methods is concerned, it has already been reported that EC series shows a good agreement with integration only for the first two peak moments (*i.e.*, m, σ) [16]. Therefore, only retention time values are compared in Table II–III. From the data thus far presented, it can therefore be concluded that, once a complete EC peak shape analysis has been used to define the NCL, EC fitting and integration are consistent. Determination of quantities such as the polymer MW can thus be performed either by integration or by EC fitting once the onset of nonlinearity for the analysis of the specific polymer/solvent system has been completely exploited. It must, however, be noted that only the EC approach is able to unambiguosly single out nonlinearity effects, whereas numerical integration only relies on its own parameters (m and σ) which can, moreover, be biased. It can, thus, be concluded that EC series method is a general numerical approach for peak shape and retention analysis in ThFFF. Several are, indeed, the reported topics of ThFFF analysis which would generally require an optimized approach in order to obtain meaningful measurements from retention parameters (*e.g.*, sample load, sample concentration and relaxation procedure). All such aspects

would require separate handling. EC series approach is here demonstrated to surely be superior to either a graphical analysis or to classical integration methods.

Acknowledgments

The authors are grateful to ENICHEM S.p.A. for having made available the complete ThFFF apparatus for the data presented and for having supported in part this work.

SYMBOL TABLE

A peak area (Equations (1) and (4))
A, b polymer/solvent constants at a given temperature [7] (Equations (17) and (18))
ANR approximation-to-noise ratio parameter (Equation (7))
c_0 sample concentration near the accumulation wall
c^* critical sample concentration at the onset of the semi-dilute regime
c_{inj} injected sample concentration
$CV\%$ percent coefficient of variation (Equations (6) and (7))
D ordinary diffusion coefficient [1] (Equations (16) and (17))
D_T thermal diffusion [1] (Equations (16) and (18))
E peak excess (Equation (9))
EC Edgeworth-Cramér series
H plate height
K EC series expansion order
K_{max} EC series expansion order of the best fitting
l solute mean layer thickness (Equation (14))
m peak mean
m_3, m_4 third and fourth peak central moment (Equations (8) and (9))
NCL necessary conditions for linearity
n_p number of parameters for a minimization pattern (Equation (6))
N_p number of points for a minimization pattern (Equation (6))
PS polystyrene
$Q_\upsilon(-Z)$ EC series terms of order υ (Equation (3))
R retention ratio (Equations (13) and (15))

$r_K(x)$ EC series remainder [13] (Equations (2))
S peak skewness (Equations (8), (11) and (12))
S.G. Savitsky-Golay smoothing
S/N signal-to-noise ratio [21] (Equation (7))
t_0 dead time (Equation (13))
t_{max} elution time of the peak maximum (Equation (12))
t_r retention time defined as elution time of the peak barycenter (Equation (13))
V_0 dead volume (Equation (13))
V_r elution volume (Equation (13))
w channel thickness (Equation (14))
x normalized time variable
X_0 mode normalized coordinate (Equations (10) and (11))
$y(x)$ normalized peak shape function (frequency function) (Equations (1) and (2))
$y_K(x)$ EC series expansion developed up to the Kth term (Equations (2), (3) and (4))
$Y(x)_{cal,K}$, $Y_{cal,K,i}$ EC fitted peak profile (Equations (4) and (5))
$Y_{sp}(x)$ experimental peak profile (Equation (1))
$Y_{sp,i}$ digitized peak profile (Equation (5))
Y_{max} peak height (Equation (5))
$Z(x)$ Gaussian function (Equation (3))
γ_v EC series cumulant coefficients [13] (Equations (3) and (5))
$\Delta_{K,i}$% fitting residuals (Equations (5) and (6))
$(\Delta t/t_{max})$% percent retention time error (Equation (12))
$(\Delta M/M)$% relative error on MW determination (Equation (19))
Δt difference between elution time of peak maximum and retention time (Equation (10))
ΔT temperature difference across the channel (Equations (16) and (18))
λ dimensionless solute mean layer thickness (Equations (14), (15), (16), and (18))
μ sample polydispersity
σ peak standard deviation

References

[1] H. G. Barth and R. B. Flippen, *Anal. Chem.*, **67**, 257R (1995).
[2] J. C. Giddings In *Size Exclusion Chromatography*; B. J. Hunt and S. R. Holding, Eds.; Blackie and Son: Glasgow, UK, 1989; Chapter 8, p 191.
[3] G. H. Thompson, M. N. Myers and J. C. Giddings, *Sep. Sci.*, **2**, 797 (1967).

[4] J. C. Giddings, *Unified Separation Science*; J. Wiley & Sons: New York, 1991; Chapter 7.
[5] J. J. Kirkland and W. W. Yau, *Macromolecules*, **18**, 2305 (1985).
[6] J. J. Kirkland, S. W. Rementer, and W. W. Yau, *Anal. Chem.*, **68**, 610 (1988).
[7] M. E. Schimpf and J. C. Giddings, *J. Polym. Sci.*, **27**, 1317 (1989).
[8] W. W. Yau, J. J. Kirkland and D. D. Bly, *Modern Size-Exclusion Liquid Chromatography*; J. Wiley & Sons: New York, 1979; Chapter 9.
[9] J. J. Kirkland and S. W. Rementer, *Anal. Chem.*, **64**, 904 (1992).
[10] M. E. Schimpf, M. N. Myers, and J. C. Giddings, *J. Appl. Polym. Sci.*, **33**, 117 (1987).
[11] K. D. Caldwell, S. L. Brimhall, Y. Gao, and J. C. Giddings, *J. Appl. Polym. Sci.*, **36**, 703 (1988).
[12] M. N. Myers, K. D. Caldwell, and J. C. Giddings, *Sep. Sci.*, **9**, 47 (1974).
[13] P. Reschiglian, G. Blo, and F. Dondi, *Anal. Chem.*, **63**, 120 (1991).
[14] F. Dondi, A. Betti, G. Blo, and C. Bighi, *Anal. Chem.*, **53**, 496 (1981).
[15] F. Dondi, *Anal. Chem.*, **54**, 473 (1982).
[16] F. Dondi and F. Pulidori, *J. Chromatogr.*, **284**, 293 (1984).
[17] F. Dondi and M. Remelli, *J. Chromatogr.*, **315**, 67 (1984).
[18] F. Dondi and M. Remelli, *J. Phys. Chem.*, **90**, 1885 (1986).
[19]. F. Dondi, G. Blo, M. Remelli and P. Reschiglian In *Theoretical Advancement in Chromatography and Related Separation Techniques*; F. Dondi and G. Guiochon, Eds.; NATO ASI Series; Kluwer Academic: Dordrecht, The Netherlands, 1992; p 173.
[20] F. Y. Edgeworth, *Proc. Cambridge Philos. Soc.*, **20**, 36 (1905).
[21] J. P. Foley and J. G. Dorsey, *Chromatographia*, **18**, 503 (1984).
[22] M. Remelli, G. Blo, F. Dondi, M. C. Vidal-Madjar, and G. Guiochon, *Anal. Chem.*, **61**, 1489 (1983).
[23] G. Blo, M. Remelli, F. Pedrielli, L. Balconi, F. Sigon, and F. Dondi, *J. Chromatogr.*, **556**, 249 (1991).
[24] H. Cramér, *Mathematical Methods of Statistics*; Princeton University: Princeton, 1957; 7th ed., Chapter 17.
[25] M. Martin and R. Reynaud, *Anal. Chem.*, **52**, 2293 (1980).
[26] *Programmer's Manual, 4th ed.*; IBM Application Program, System-/360 Scientific Subroutine Package (360-CM-03X) Version III; IBM Technical Publications Department: White Plains, 1968; p. 225.
[27] J. Janca and M. Martin, *Chromatographia*, **34**, 125 (1992).
[28] K. Nachtigall and G. Meyerhoff, *Makromol. Chem.*, **33**, 85 (1959).
[29] G. Meyerhoff and K. Nachtigall, *J. Polym. Sci.*, **57**, 227 (1962).
[30] B. Rauch and G. Meyerhoff, *Z. Phys. Chem.*, **65**, 1 (1969).
[31] P. N. Pusey, J. M. Vaughan, and G. Williams, *J. Chem. Soc. Faraday Trans.*, **II 70**, 1696 (1974).
[32] J. Roots, B. Nyström, L.-O. Sundelöf, and B. Porsch, *Polymer* **20**, 337 (1979).
[33] V. Petrus, B. Porsch, B. Nyström, and L.-O. Sundelöf, *Makromol. Chem.*, **183**, 1279 (1982).
[34] M. Hoyos and M. Martin, *Anal. Chem.*, **66**, 1718 (1994).
[35] M. E. Hansen, J. C. Giddings, and R. Beckett, *J. Colloid Interface Sci.*, **132**, 300 (1989).
[36] J. D. Hoffman and B. H. Zimm, *J. Polym. Sci.*, **15**, 405 (1955).
[37] F. C. Whitmore, *J. Appl. Phys.*, **31**, 1858 (1960).
[38] G. Meyerhoff and B. Rauch, *Makromol. Chem.*, **127**, 214 (1969).
[39] P. Debye and A. M. Bueche In *High Polymer Physics*; H. A. Robinson, Ed.; Chemical Publishing: Brooklyn, 1948; p 497.
[40] A. Litzén and K.-G. Wahlund, *J. Chromatogr.*, **548**, 393 (1991).
[41] A. Carlshaf and J. A. Jönsson, *Sep. Sci. Technol.*, **28**, 1191 (1993).